AD-A116 586 OHIO STATE UNIV COLUMBUS ELECTROSCIENCE LAB F/G 9/5
ADAPTIVE ARRAY BEHAVIOR WITH SINUSOIDAL ENVELOPE MODULATED INTE--ETC(U)
MAR 82 A S AL-RUWAIS, R T COMPTON N00019-81-C-0093
UNCLASSIFIED ESL-713603-5 NL

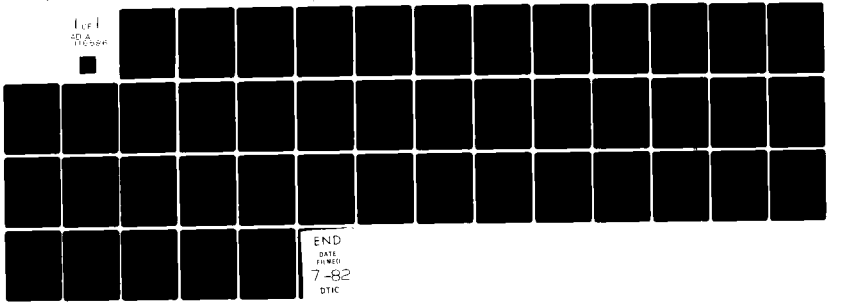

(12)

OSU

The Ohio State University

ADAPTIVE ARRAY BEHAVIOR WITH SINUSOIDAL ENVELOPE MODULATED [redacted] INTERFERENCE

Abdulaziz S. Al-Ruwais and R.T. Compton, Jr.

The Ohio State University

ElectroScience Laboratory

Department of Electrical Engineering
Columbus, Ohio 43212

Technical Report ESL-713603-5

Contract N00019-81-C-0093

March 1982

Naval Air Systems Command
Washington, D.C. 20361

50272-101

REPORT DOCUMENTATION PAGE	1. REPORT NO. AD-A116 556	2.	3. Recipient's Accession No

4. Title and Subtitle

Adaptive Array Behavior with Sinusoidal Envelope Modulated Interference

5. Report Date: March 1982

6.

7. Author(s): Abdulaziz S. Al-Ruwais and R.T. Compton, Jr.

8. Performing Organization Rept. No: 713603-5

9. Performing Organization Name and Address

The Ohio State University
ElectroScience Laboratory
Department of Electrical Engineering
Columbus, Ohio 43212

10. Project/Task/Work Unit No.

11. Contract(C) or Grant(G) No
(C) N00019-81-C-0093
(G)

12. Sponsoring Organization Name and Address

Naval Air Systems Command
Washington, D.C. 20361

13. Type of Report & Period Covered: Technical Report

14.

15. Supplementary Notes

16. Abstract (Limit: 200 words)

The behavior of an LMS adaptive array with modulated interference is described. An interference signal with sinusoidal, double-sideband, suppressed-carrier modulation is assumed. It is shown that such interference causes the array to modulate the desired signal envelope but not its phase. The amount of the desired signal modulation is determined as a function of signal arrival angles and powers and the modulation frequency of the interference.

Such interference also causes the array output signal-to-interference-plus-noise ratio (SINR) to vary with time. However, it is shown that when the desired signal is a digital communication signal, the averaged bit error probability is essentially the same as for CW interference.

17. Document Analysis a. Descriptors

Adaptive Arrays
Interference Rejection
Antennas

b. Identifiers/Open-Ended Terms

DISTRIBUTION UNLIMITED

c. COSATI Field/Group

18. Availability Statement: APPROVED FOR PUBLIC RELEASE; DISTRIBUTION UNLIMITED

19. Security Class (This Report): Unclassified
20. Security Class (This Page): Unclassified

21. No. of Pages: 40
22. Price

(See ANSI-Z39.18) See Instructions on Reverse

OPTIONAL FORM 272 (4-77)
(Formerly NTIS-35)
Department of Commerce

TABLE OF CONTENTS

LIST OF FIGURES

Page

I. INTRODUCTION

Adaptive arrays based on the LMS algorithm of Widrow, et al[1] can be used to protect communication systems from interference. These antennas optimize reception of a desired signal while simultaneously nulling interference. For a given set of incoming signals, the LMS array yields the maximum attainable signal-to-interference-plus-noise ratio (SINR) at the array output[2,3].

Most studies of adaptive array performance have assumed interference signals that have constant power. However, a modulated interference signal may be more difficult for the array to null. If the modulation rate of the interference is close to the natural response rate of the array, such a signal may keep the array in a continual transient state.

In a previous paper[4], one of the authors examined the performance of an LMS array with pulsed interference. It was shown, for example, that when the array is used to receive a differential phase-shift keyed (DPSK) signal, pulsed interference can increase the bit error probability more than CW interference does. However, the increase due to the pulse modulation is small, and occurs only if the pulse repetition rate, duty cycle and interference power are all properly chosen. Otherwise, pulsed interference has less effect than CW interference.

In this report, we study the effect of another type of envelope modulated interference on the LMS array. Specifically, we consider an interference signal with double-sideband, suppressed carrier, sinusoidal envelope modulation. This type of signal has been chosen for two reasons. First, such interference contains a spectral line on each side of the desired signal frequency; by changing the interference modulation frequency, we can explore the frequency response of the LMS loop. (The LMS loop is nonlinear in the

input signals.) Second, such modulation yields a system of differential equations for the array weights that can be solved. In general, an interference signal with arbitrary modulation leads to an intractable mathematical problem.

As we shall show, modulated interference of this type has two effects on the array. First, it causes the array to modulate the desired signal envelope (but not its phase!). Second, it makes the output SINR from the array vary with time. However, it turns out that this SINR variation causes almost no change in average bit error probability (as compared with CW interference) when the array is used in a digital communication system.

In section II of the report we establish notation, define the interference signal and solve for the weight response of the adaptive array. In section III we present calculated results obtained from the equations in section II and discuss the effect of each interference signal parameter on the array performance. Section IV contains the conclusions.

II. FORMULATION OF THE PROBLEM

Consider an LMS adaptive array[1] consisting of three isotropic elements a half wavelength apart, as shown in Figure 1. The analytic signal $\tilde{x}_j(t)$ from element j is multiplied by complex weight w_j and then summed to produce the array output $\tilde{s}(t)$. The error signal $\tilde{\epsilon}(t)$, which is the difference between the array output signal and the reference signal $\tilde{r}(t)$, forms the input to a feedback system that adjusts the w_j. In the LMS array, the weights satisfy the system of equations[1,5]

$$\frac{dW}{dt} + k\Phi W = kS, \tag{1}$$

where $W=(w_1, w_2, w_3)^T$ is the weight vector, Φ is the covariance matrix,

$$\Phi = E[X^*X^T], \tag{2}$$

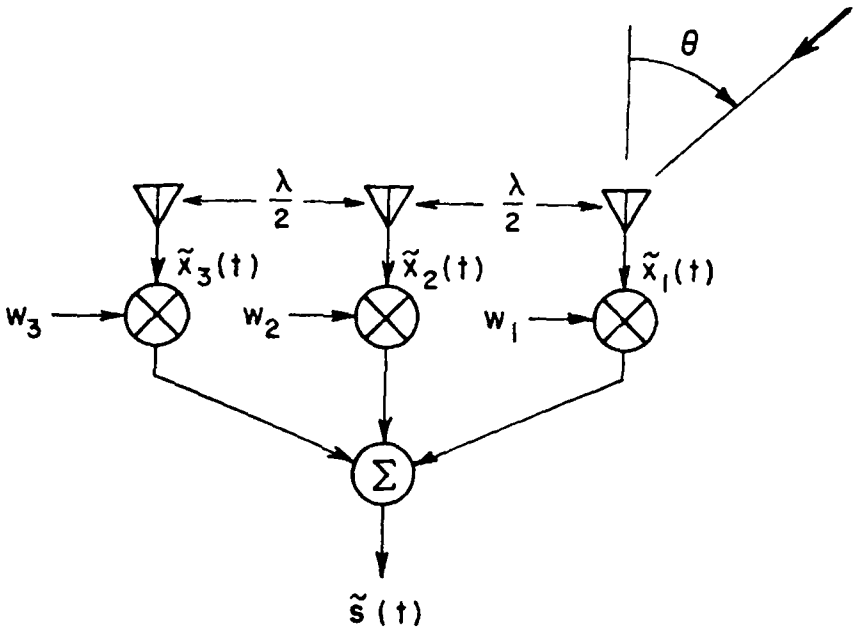

Figure 1. A Three-Element LMS Array

S is the reference correlation vector,

$$S = E[X^{*}\tilde{r}(t)], \tag{3}$$

and k is the LMS loop gain. In these equations, X is the signal vector,

$$X = [\tilde{x}_1(t), \tilde{x}_2(t), \tilde{x}_3(t)]^{T}, \tag{4}$$

T denotes transpose, * complex conjugate, and E[•] expectation.

We assume that a desired and an interference signal are incident on the array and that thermal noise is also present in each element signal. The signal vector then contains three terms,

$$X = X_d + X_i + X_n, \tag{5}$$

where X_d, X_i and X_n are the desired, interference and thermal noise vectors, respectively.

Specifically, we assume a CW desired signal is incident from angle θ_d relative to broadside. (θ is defined in Figure 1.) The desired signal vector is then

$$X_d = A_d e^{j(\omega_o t+\psi_d)} U_d, \tag{6}$$

where A_d is the amplitude, ω_o is the carrier frequency, ψ_d is the carrier phase angle, and U_d is a vector containing the interelement phase shifts,

$$U_d = (1, e^{-j\phi_d}, e^{-j2\phi_d})^{T}, \tag{7}$$

with

$$\phi_d = \pi \sin\theta_d. \tag{8}$$

We assume ψ_d to be a random variable uniformly distributed on $(0,2\pi)$.

Next, we assume an envelope modulated interference signal as shown in Figure 2, arriving from angle θ_i. The interference signal vector is then

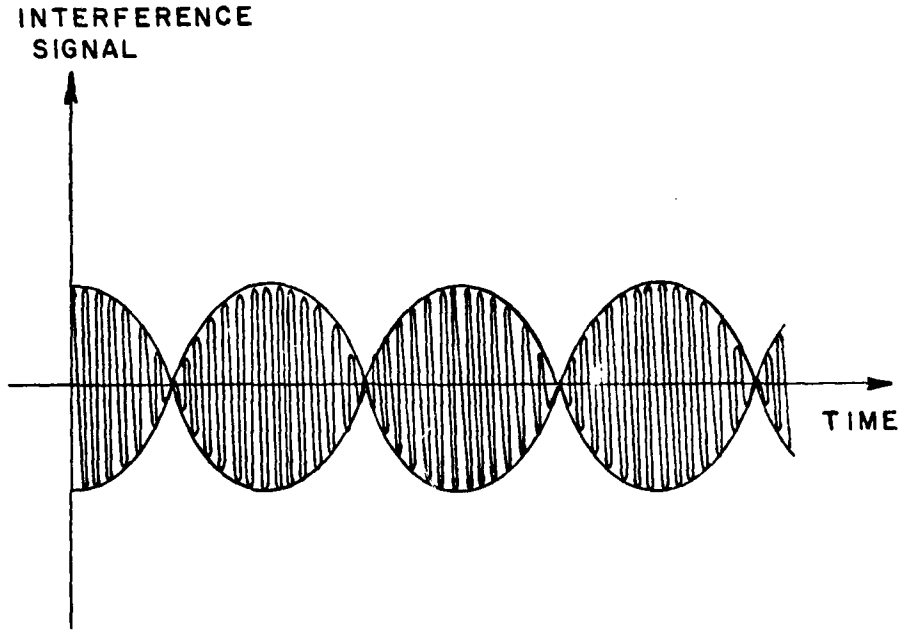

Figure 2. Sinusoidally Modulated Interference

$$X_i = e^{j(\omega_0 t+\psi_i)} \begin{matrix} a_i(t) \\ a_i(t-T_i)e^{-j\omega_0 T_i} \\ a_i(t-2T_i)e^{-j2\omega_0 T_i} \end{matrix}, \tag{9}$$

where $a_i(t)$ is the envelope modulation as received on element 1, ψ_i is the carrier phase angle, and T_i is the interelement time delay given by

$$T_i = \frac{\pi}{\omega_0}\sin\theta_i. \tag{10}$$

We assume ψ_i is a random variable uniformly distributed on $(0,2\pi)$ and statistically independent of ψ_d.

In this paper, we shall study the case where $a_i(t)$ is a simple sinusoid,

$$a_i(t) = A_i\cos\omega_m t, \tag{11}$$

with A_i and ω_m the amplitude and frequency, respectively. I.e., the interference is a double-sideband, suppressed carrier signal. As mentioned above, we have chosen this type of modulation for two reasons. First, this signal has two spectral lines, one on each side of the desired signal frequency. By varying ω_m we can change the separation between the desired and interference spectral lines and examine the frequency response of the array weights. Second, this type of modulation leads to a tractable mathematical problem. More complicated modulations yield differential equations for the weight vector that are more difficult to solve.*

We shall assume the frequency ω_m in (11) is very small compared to the carrier frequency ω_0. Under this condition the time delay T_i represents a negligible delay in the modulation envelope, so the modulation on each element signal is essentially the same,

$$a_i(t) \simeq a_i(t-T_i) \simeq a_i(t-2T_i). \tag{12}$$

*Specifically, the modulation in (11) yields a 3-term recursion relation in Eq.(57) below. If, for example, $a_i(t)$ is assumed to contain a carrier term in addition to the two sidebands, a 5-term recursion relation results instead of (57). The weight differential equation then cannot be solved by the methods presented here.

In this case X_i reduces to

$$X_i = A_i \cos\omega_m t e^{j(\omega_0 t + \psi_i)} U_i, \tag{13}$$

where

$$U_i = [1,\ e^{-j\phi_i},\ e^{-j2\phi_i}]^T, \tag{14}$$

with

$$\phi_i = \pi \sin\theta_i. \tag{15}$$

Finally, we assume the thermal noise vector is given by

$$X_n = [\tilde{n}_1(t),\ \tilde{n}_2(t),\ \tilde{n}_3(t)]^T, \tag{16}$$

where the $\tilde{n}_j(t)$ are zero-mean, gaussian thermal noise voltages, all statistically independent of each other, and each of power σ^2. Thus,

$$E[\tilde{n}_j^*(t)\tilde{n}_k(t)] = \sigma^2 \delta_{jk}, \tag{17}$$

with δ_{ij} the Kronecker delta. Also, we assume the $\tilde{n}_j(t)$ are statistically independent of ψ_d and ψ_i.

Under these assumptions, the covariance matrix in (2) becomes

$$\Phi = \Phi_d + \Phi_i + \Phi_n, \tag{18}$$

where

$$\Phi_d = A_d^2 U_d^* U_d^T, \tag{19}$$

$$\Phi_i = A_i^2 \cos^2\omega_m t U_i^* U_i^T$$

$$= (1/2) A_i^2 [1+\cos 2\omega_m t] U_i^* U_i^T, \tag{20}$$

and

$$\Phi_n = \sigma^2 I, \tag{21}$$

where I is the identity matrix.

To compute the reference correlation vector S in (3), we must first define the reference signal $\tilde{r}(t)$. In practice, the reference signal is usually derived from the array output[6,7]. It must be a signal correlated with the desired signal and uncorrelated with the interference. Here we assume the reference signal to be

$$\tilde{r}(t) = A_r e^{j(\omega_o t+\psi_d)}. \tag{22}$$

Eq.(3) then yields

$$S = A_r A_d U_d^*. \tag{23}$$

Eqs.(18)-(21) and (23) can now be inserted in (1) to give the differential equation for the weight vector W,

$$\frac{dW}{dt} + k[\sigma^2 I + A_d^2 U_d^* U_d^T + (1/2)A_i^2(1+\cos 2\omega_m t)U_i^* U_i^T]W = kA_r A_d U_d^*. \tag{24}$$

Before attempting to solve (24), it is helpful to put it in normalized form. First, dividing by $k\sigma^2$ gives

$$\frac{dW(t')}{dt'} + [I + \xi_d U_d^* U_d^T + (1/2)\xi_i(1+\cos 2\omega_m' t')U_i^* U_i^T]W(t') = \frac{A_r}{\sigma}\sqrt{\xi_d}U_d^*, \tag{25}$$

where

$\xi_d = \frac{A_d^2}{\sigma^2}$ = input signal-to-noise ratio (SNR) per element,

$\xi_i = \frac{A_i^2}{\sigma^2}$ = peak input interference-to-noise ratio (INR) per element.

and where we have also used normalized time and frequency variables,

$\omega_m' = \omega_m/k\sigma^2$ = normalized modulation frequency,

$t' = k\sigma^2 t$ = normalized time.

Next we note that the constant A_r/σ on the right side of (25) will just appear as a scale factor in the solution for W. It has no effect on the array output signal-to-noise ratios to be computed below. Hence we arbitrarily set $A_r/\sigma=1$ to eliminate it. Finally, by defining

$$\Phi_o = I + \xi_d U_d^* U_i^T + (1/2)\xi_i U_i^* U_i^T, \tag{26}$$

we can write (25) in the form,

$$\frac{dW(t')}{dt'} + [\Phi_o+(1/2)\xi_i\cos(2\omega_m't')U_i^*U_i^T]W(t') = \sqrt{\xi_d}U_d^*. \tag{27}$$

Eq.(27) is a linear vector differential equation with a constant source term on the right but with periodic coefficients. The general properties of such differential equations have been described by D'Angelo[8]. He has shown that the solution for W(t') will be a periodic function of time once the initial transients have died out.

In this paper, we shall not consider the initial transient behavior, but shall concentrate on the periodic steady-state solution for W(t'). Once W(t') is periodic, it can be represented as a Fourier series

$$W(t') = \sum_{n=-\infty}^{\infty} C_n e^{j2n\omega_m't'}, \tag{28}$$

where C_n is a vector Fourier coefficient. Substituting (28) into (27), replacing $\cos(2\omega_m't')$ with exponentials, and collecting terms with the same frequency, we find that the coefficients C_n must satisfy

$$\sum_{n=-\infty}^{\infty} [(\Phi_o+j2n\omega_m'I)C_n+(1/4)\xi_i U_i^*U_i^T(C_{n-1}+C_{n+1})]e^{j2n\omega_m't'} = \sqrt{\xi_d}U_d^*. \tag{29}$$

Enforcing this equation for each frequency component separately gives, for n=0,

$$\Phi_o C_o+(1/4)\xi_i U_i^*U_i^T(C_{-1}+C_1) = \sqrt{\xi_d}U_d^*, \tag{30}$$

and for $n \neq 0$,

$$(\Phi_0 + j2n\omega_m' I)C_n + (1/4)\xi_i U_i^* U_i^T (C_{n-1} + C_{n+1}) = 0. \quad (31)$$

These equations may be solved for the C_n by expressing each C_n in terms of its components parallel and perpendicular to the vector U_i^*. To do this, we first form a set of three orthonormal basis vectors* as follows. Let e_1 be a unit vector parallel to U_i^*,

$$e_1 = \frac{U_i^*}{\sqrt{U_i^T U_i^*}}, \quad (32)$$

and let e_2 and e_3 be unit vectors perpendicular to each other and to e_1, i.e.,

$$e_j^\dagger e_k = \delta_{jk}, \quad (33)$$

(where $\dagger$ is conjugate transpose). In particular, let e_2 be in the plane defined by U_d^* and U_i^*,

$$e_2 = \zeta[U_d^* - \kappa U_i^*], \quad (34)$$

where ζ and κ are constants. Enforcing the orthogonality condition $e_1^\dagger e_2 = 0$ and choosing ζ so e_2 has unit magnitude yields,

$$e_2 = \frac{1}{\sqrt{U_d^T U_d^* - \frac{U_i^T U_d^*}{U_i^T U_i^*}}} \left[U_d^* - \frac{U_i^T U_d^*}{U_i^T U_i^*} U_i^*\right]. \quad (35)$$

e_3 is easily found from e_1 and e_2 but will not be needed in the sequel, so we shall not compute it explicitly.

Each coefficient C_n may be written in terms of the unit vectors e_k as

$$C_n = \sum_{k=1}^{3} \alpha_{n,k} e_k, \quad (36)$$

where the $\alpha_{n,k}$ are scalar coefficients. $\alpha_{n,k}$ is the component of C_n along the unit vector e_k.

*The array has 3 elements, so $W(t')$ and C_n each have 3 components. Hence 3 basis vectors are needed to span the space for C_n.

Substituting Eq.(36) into (30) and (31) and utilizing the fact that $U_i^T e_j = 0$ for $j \neq 1$, we obtain

$$\Phi_o \sum_{k=1}^{3} \alpha_{0,k} e_k + (1/4)\xi_i |U_i^*|^2 (\alpha_{-1,1} + \alpha_{1,1}) = \sqrt{\xi_d} U_d^*, \quad (37)$$

and

$$\sum_{k=1}^{3} \alpha_{n,k} (\Phi_o + j2n\omega_m' I) e_k + (1/4)\xi_i |U_i^*|^2 (\alpha_{n-1,1} + \alpha_{n+1,1}) = 0, \; n \neq 0. \quad (38)$$

Multiplying these two equations by $e_j^\dagger$ on the left gives

$$\sum_{k=1}^{3} \alpha_{0,k} \beta_{jk} + (1/4)\xi_i |U_i^*|^2 (\alpha_{-1,1} + \alpha_{1,1}) \delta_{j1} = \sqrt{\xi_d} e_j^\dagger U_d^*, \quad (39)$$

and

$$\sum_{k=1}^{3} \alpha_{n,k} (\beta_{jk} + j2n\omega_m' \delta_{jk}) + (1/4)\xi_i |U_i^*|^2 (\alpha_{n-1,1} + \alpha_{n+1,1}) \delta_{j1} = 0, \; n \neq 0, \quad (40)$$

where we have defined

$$\beta_{jk} = e_j^\dagger \Phi_o e_k. \quad (41)$$

Eqs.(39) and (40) hold for $1 \leq j \leq 3$. THe values of β_{jk} are readily found by substituting (26), (32) and (35) into (41) and making use of (33) for e_3. The results are

$$\beta_{11} = 1 + \xi_d \frac{|U_i^T U_d^*|^2}{U_i^T U_i^*} + (1/2)\xi_i U_i^T U_i^*, \quad (42)$$

$$\beta_{22} = 1 + \xi_d \rho, \quad (43)$$

$$\beta_{12} = \beta_{21}^* = \xi_d \sqrt{\rho} \frac{U_i^T U_d^*}{\sqrt{U_i^T U_i^*}}, \quad (44)$$

$$\beta_{13} = \beta_{31} = \beta_{23} = \beta_{32} = 0, \quad (45)$$

and

$$\beta_{33} = 1, \quad (46)$$

where

$$\rho = U_d{}^T U_d{}^* - \frac{|U_i{}^T U_d{}^*|^2}{U_i{}^T U_i{}^*}. \tag{47}$$

In addition, one finds

$$e_1{}^\dagger U_d{}^* = \frac{U_i{}^T U_d{}^*}{\sqrt{U_i{}^T U_i{}^*}}, \tag{48}$$

$$e_2{}^\dagger U_d{}^* = \sqrt{\rho}, \tag{49}$$

and

$$e_3{}^\dagger U_d{}^* = 0. \tag{50}$$

Our problem now is to solve (39) and (40) for the $\alpha_{n,k}$. We may do this as follows. Writing out (39) and (40) for $1 \leq j \leq 3$ gives the six equations,

$$\beta_{11}\alpha_{0,1}+\beta_{12}\alpha_{0,2}+(1/4)\xi_i|U_i{}^*|^2(\alpha_{-1,1}+\alpha_{1,1})=\sqrt{\xi_d}e_1{}^\dagger U_d{}^*, \tag{51}$$

$$\beta_{21}\alpha_{0,1}+\beta_{22}\alpha_{0,2}=\sqrt{\xi_d}e_2{}^\dagger U_d{}^*, \tag{52}$$

$$\alpha_{0,3}=0, \tag{53}$$

$$(\beta_{11}+j2n\omega_m')\alpha_{n,1}+\beta_{12}\alpha_{n,2}=-(1/4)\xi_i|U_i{}^*|^2(\alpha_{n-1,1}+\alpha_{n+1,1}), \tag{54}$$

$$\beta_{21}\alpha_{n,1}+(\beta_{22}+j2n\omega_m')\alpha_{n,2}=0, \tag{55}$$

and

$$\alpha_{n,3} = 0, \tag{56}$$

where the last three equations hold for $n \neq 0$. Solving (54) and (55) for $\alpha_{n,1}$ and $\alpha_{n,2}$ yields

$$\alpha_{n,1} = -\gamma_n(\alpha_{n-1,1}+\alpha_{n+1,1}) \tag{57}$$

and

$$\alpha_{n,2} = -\frac{\beta_{12}^*}{(\beta_{22}+j2n\omega_m')}, \tag{58}$$

where

$$\gamma_n = \frac{\xi_i(\beta_{22}+j2n\omega_m')|U_i^*|^2}{4[(\beta_{11}+j2n\omega_m')(\beta_{22}+j2n\omega_m')-|\beta_{12}|^2]}. \tag{59}$$

Eq.(58) allows one to calculate $\alpha_{n,2}$ from $\alpha_{n,1}$, so the problem is reduced to determining the $\alpha_{n,1}$. To find the $\alpha_{n,1}$, we must solve (57).

Eq.(57) is a three-term recursion relation for the coefficients $\alpha_{n,1}$. Given $\alpha_{n,1}$ for two successive n, one could calculate all the remaining $\alpha_{n,1}$ from (57). However, if one starts from arbitrary initial values for the $\alpha_{n,1}$, one finds that in general $\alpha_{n,1}$ will not approach zero as $n\to\pm\infty$, so the series in (28) will not converge. Only the correct initial values of $\alpha_{n,1}$ will cause the series to converge.*

To determine the correct initial values for the $\alpha_{n,1}$, we manipulate (57) into two forms,

$$\frac{\alpha_{n,1}}{\alpha_{n-1,1}} = \frac{-1}{\frac{1}{\gamma_n}+\frac{\alpha_{n+1,1}}{\alpha_{n,1}}} \quad \text{for } n>0, \tag{60}$$

and

$$\frac{\alpha_{n,1}}{\alpha_{n+1,1}} = \frac{-1}{\frac{1}{\gamma_n}+\frac{\alpha_{n-1,1}}{\alpha_{n,1}}} \quad \text{for } n<0. \tag{61}$$

Consider first the behavior of $\alpha_{n,1}$ for large positive n. Eq.(59) shows that for large n,

$$\frac{1}{\gamma_n} \to \frac{8jn\omega_m'}{\xi_i|U_i^*|^2}. \tag{62}$$

*The situation here is similar to that encountered in solving the Mathieu equation[9].

Hence, we conclude from (60) that $\alpha_{n,1}/\alpha_{n-1,1}$ will approach zero as $n\to\infty$, as long as the next term, $\alpha_{n+1,1}/\alpha_{n,1}$, also approaches zero. Therefore, the approach we shall take for finding the $\alpha_{n,1}$ is to assume $\alpha_{N+1,1}/\alpha_{N,1}=0$ for some suitably large N and then use (60) to compute $\alpha_{n,1}/\alpha_{n-1,1}$ iteratively, starting at n=N and working down. This procedure yields $\alpha_{1,1}/\alpha_{0,1}$ as a continued fraction:

$$\frac{\alpha_{1,1}}{\alpha_{0,1}} = \cfrac{-1}{\frac{1}{\gamma_1}+\cfrac{-1}{\frac{1}{\gamma_2}+\cfrac{-1}{\frac{1}{\gamma_3}+\cfrac{-1}{\ddots\;+\cfrac{-1}{\frac{1}{\gamma_N}}}}}}, \tag{63}$$

where the continued fraction terminates at γ_N. A similar continued fraction may be found for $\alpha_{-1,1}/\alpha_{0,1}$ from (61). However, since

$$\gamma_{-n} = \gamma_n^*, \tag{64}$$

the result is just

$$\frac{\alpha_{-1,1}}{\alpha_{0,1}} = \left\{\frac{\alpha_{1,1}}{\alpha_{0,1}}\right\}^*, \tag{65}$$

Hence it is sufficient to evaluate (63) for $\alpha_{1,1}/\alpha_{0,1}$ and then use (65) to find $\alpha_{-1,1}/\alpha_{0,1}$.

Suppose the continued fraction in (63) yields a value r:

$$\frac{\alpha_{1,1}}{\alpha_{0,1}} = r. \tag{66}$$

We may then substitute

$$\alpha_{1,1} = r\alpha_{0,1}, \tag{67}$$

and

$$\alpha_{-1,1} = r^*\alpha_{0,1}, \tag{68}$$

into (51) to obtain

$$[\beta_{11}+(1/4)\xi_i|U_i^*|^2(r+r^*)]\alpha_{0,1}+\beta_{12}\alpha_{0,2}=\sqrt{\xi_d}e_1^\dagger U_d^*. \tag{69}$$

Solving (69) and (52) simultaneously yields

$$\alpha_{0,1} = \frac{\sqrt{\xi_d}(\beta_{22}e_1^\dagger U_d^*-\beta_{12}e_2^\dagger U_d^*)}{[\beta_{11}+(1/2)\xi_i|U_i^*|^2\mathrm{Re}(r)]\beta_{22}-|\beta_{12}|^2}. \tag{70}$$

Once $\alpha_{0,1}$ has been computed, $\alpha_{0,2}$ may be found from (52):

$$\alpha_{0,2} = \frac{\sqrt{\xi_d}e_2^\dagger U_d^*-\beta_{21}\alpha_{0,1}}{\beta_{22}}. \tag{71}$$

We have now developed all the equations needed to compute the periodic array weights in Eq.(28). To summarize, the procedure is as follows. Starting from the signal parameters θ_d, ξ_d, θ_i, ξ_i, ω_m', we first compute the vectors U_d and U_i in (7) and (14), then the β_{jk} in (42)-(47) and the γ_n in (59). From the γ_n, we evaluate r in (66) using the continued fraction in (63). (The number of terms used in the continued fraction, N, is chosen large enough that the value of r obtained is insensitive to small changes in N.) After r is found, we use (70) to find $\alpha_{0,1}$, (71) to find $\alpha_{0,2}$, (67) to find $\alpha_{1,1}$, (57) to find $\alpha_{n,1}$ for $n\neq 0,1$, and finally (58) to find $\alpha_{n,2}$ for $n\neq 0$. From the $\alpha_{n,1}$ and $\alpha_{n,2}$ (and using $\alpha_{n,3}=0$), the C_n may be evaluated from (36) and then W(t') from (28).

The time-varying weights in (28) have two effects on array performance. First, they cause the array to modulate the desired signal. (The array becomes a time-varying, or frequency dispersive, channel[10].) Second, the array output signal-to-interference-plus-noise ratio (SINR) varies periodically with time. Our major purpose in this paper is to evaluate these two effects.

Given a time-varying weight vector W(t'), the desired signal component of the array output is

$$\tilde{s}_d(t') = A_d W^T(t') U_d e^{j(\omega_0' t'+\psi_d)}, \tag{72}$$

(where $\omega_o' = \omega_o/k\sigma^2$). To study the modulation on $\tilde{s}_d(t)$, we define

$$a_d(t')e^{j\eta_d(t')} = A_d W^T(t')U_d. \tag{73}$$

Then $a_d(t') = A_d|W^T(t')U_d|$ is the envelope modulation and $\eta_d(t') = \angle W^T(t')U_d$ is the phase modulation. Furthermore, we define $a_{dn}(t')$ to be the envelope normalized to its value in the absence of interference, i.e.,

$$a_{dn}(t') = \frac{a_d(t')}{A_d|W_o^T U_d|}, \tag{74}$$

where W_o is the steady-state weight vector that would occur without interference,

$$W_o = (\Phi_d + \Phi_n)^{-1}S. \tag{75}$$

(Φ_d, Φ_n and S are given in (19),(21) and (23).) We present our results in terms of $a_{dn}(t')$ rather than $a_d(t')$, because the effect of the interference can be determined most easily by comparing the value of $a_{dn}(t')$ with unity.

The output desired signal power is

$$P_d(t') = (1/2)E\{|\tilde{s}_d(t')|^2\} = (1/2)A_d^2|W^T(t')U_d|^2. \tag{76}$$

The output interference signal is

$$\tilde{s}_i(t') = A_i\cos(\omega_m't')e^{j(\omega_o't'+\psi_i)}W^T(t')U_i, \tag{77}$$

and the output interference power is

$$P_i(t') = (1/2)E\{|\tilde{s}_i(t')|^2\} = (1/2)A_i^2\cos^2(\omega_m't')|W^T(t')U_d|^2. \tag{78}$$

The output thermal noise power is

$$P_n(t') = \frac{\sigma^2}{2} W^\dagger(t')W(t'). \tag{79}$$

From these quantities, the output interference-to-noise ratio (INR),

$$INR = \frac{P_i(t')}{P_n(t')}, \tag{80}$$

and the output signal-to-interference-plus-noise ratio (SINR),

$$SINR = \frac{Pd(t')}{P_i(t') + P_n(t')}, \tag{81}$$

may be computed.

With this background, we now discuss the numerical results obtained from these equations.

III. RESULTS

In this section, we describe the effect of the amplitude modulated interference signal on the array. In Part A, we show typical curves of desired signal modulation, output INR and SINR as functions of time. In Parts B-E, we describe the effect of each signal parameter on the desired signal modulation. In Part F, we assume the array is used in a digital communication system and show how the bit error probability is affected by the interference.

A. Typical Waveforms

Figure 3 shows a typical curve of the normalized envelope modulation $a_{dn}(t')$ for the case $\theta_d=0°$, $\theta_i=5°$, $\xi_d=10$ dB, $\xi_i=20$ dB and $f_m'=\omega_m'/2\pi=2$.* As may be seen, there is substantial envelope modulation produced by the interference for this set of parameters.

When the phase modulation $\eta_d(t')$ is calculated, one discovers an interesting result: $\eta_d(t')$ is constant, not only for the parameters used in Figure 3, but for all values of the signal parameters. Thus, this interference does not produce phase modulation on the desired signal. A similar result was also found previously for a pulsed interference signal[4]. With pulsed interference, it is possible to prove mathematically that there is no phase modulation. For the interference considered here, we have not been able to obtain such a mathematical proof. However, calculations of $\eta_d(t')$ based on the equations in Section II consistently show that there is no phase

*Because the frequency of the periodic term in (27) is $2\omega_m'$, the envelope modulation is periodic with period $1/2f_m'=.25$. Figure 3 shows one period of the modulation.

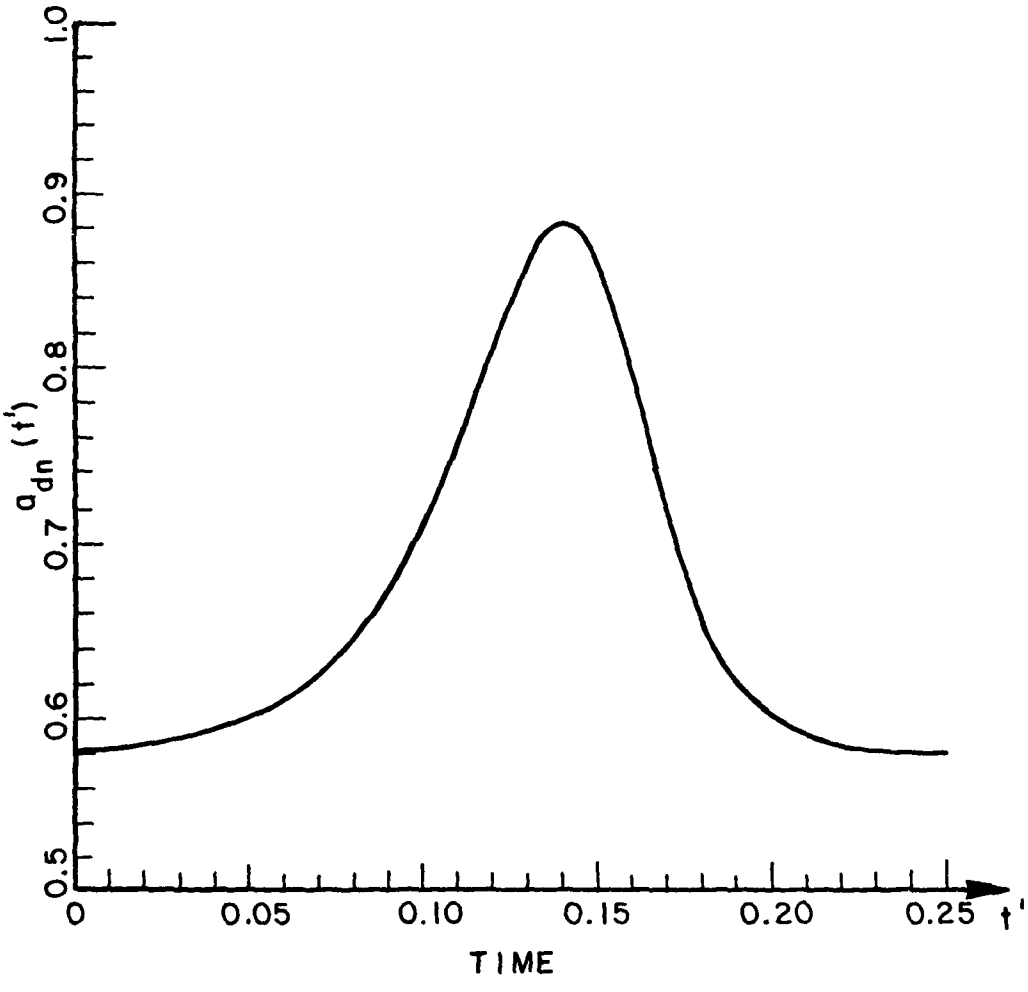

Figure 3. $a_{dn}(t')$ versus time
$\theta_d=0^o$, $\theta_i=5^o$, $\xi_d=10$ dB,
$\xi_i=20$ dB, $f_m'=2$

modulation, regardless of the values of θ_i, ξ_i or f_m'. This result is of considerable importance for adaptive arrays to be used in communication systems with phase modulation.

Next, Figures 4 and 5 show the output INR and SINR as functions of time, over one period, for the same signal parameters as in Figure 3. The sharp drop in INR in Figure 4 at t'=.125 occurs when the incoming interference power is zero. The variation in the SINR in Figure 5 is primarily due to the variation in desired signal amplitude as shown in Figure 3. However, the peak SINR occurs slightly earlier than the peak of $a_{dn}(t')$, reflecting the influence of the time-varying interference and noise powers on the SINR.

Figures 3, 4 and 5 are intended merely to illustrate typical array behavior with the interference modulation in Eq.(11). In general, the desired signal modulation and the SINR variation change substantially as the signal parameters θ_d, ξ_d, θ_i, ξ_i and f_m' are varied. In Sections B-E, we describe in detail the effect of each signal parameter on the desired signal modulation. In Section F, we show how the SINR variations affect bit error probability when the array is used in a digital communication system.

To describe the desired signal modulation, we shall define three quantities. First, we let a_{min} and a_{max} be the minimum and maximum values of $a_{dn}(t')$ during the modulation period. Then, we define

$$m = \frac{a_{max} - a_{min}}{a_{max}}. \tag{82}$$

m is the envelope variation normalized to its peak. It may be thought of as "fractional modulation", analogous to percentage modulation in AM. In Parts B-E below, we describe the effect of each signal parameter on a_{max} and m.

B. The Effect of Angle of Arrival

Desired signal modulation effects are small unless θ_i is close to θ_d. When θ_i is far from θ_d, the envelope variation m is small and the peak a_{max} is

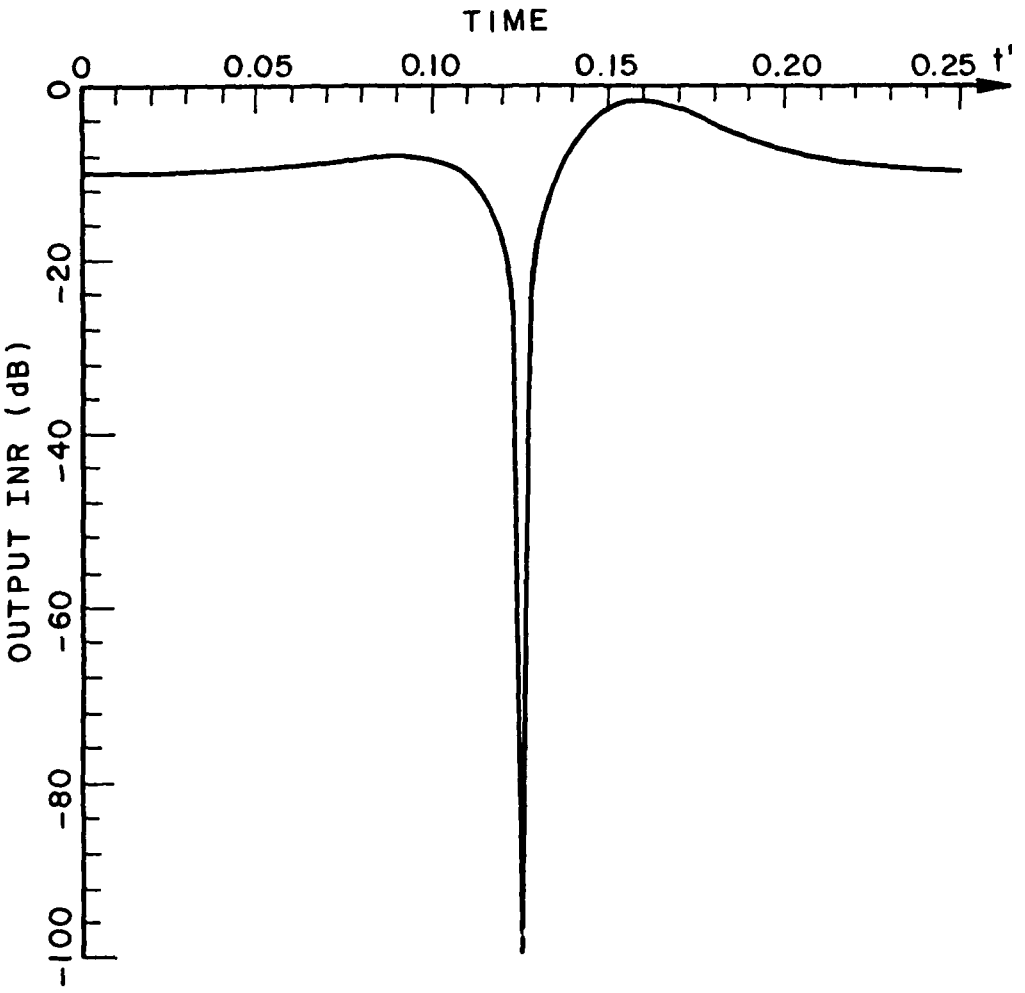

Figure 4. INR versus time
$\theta_d=0^\circ$, $\theta_i=5^\circ$, ξ_d=10 dB,
ξ_i=20 dB, $f_m'=2$

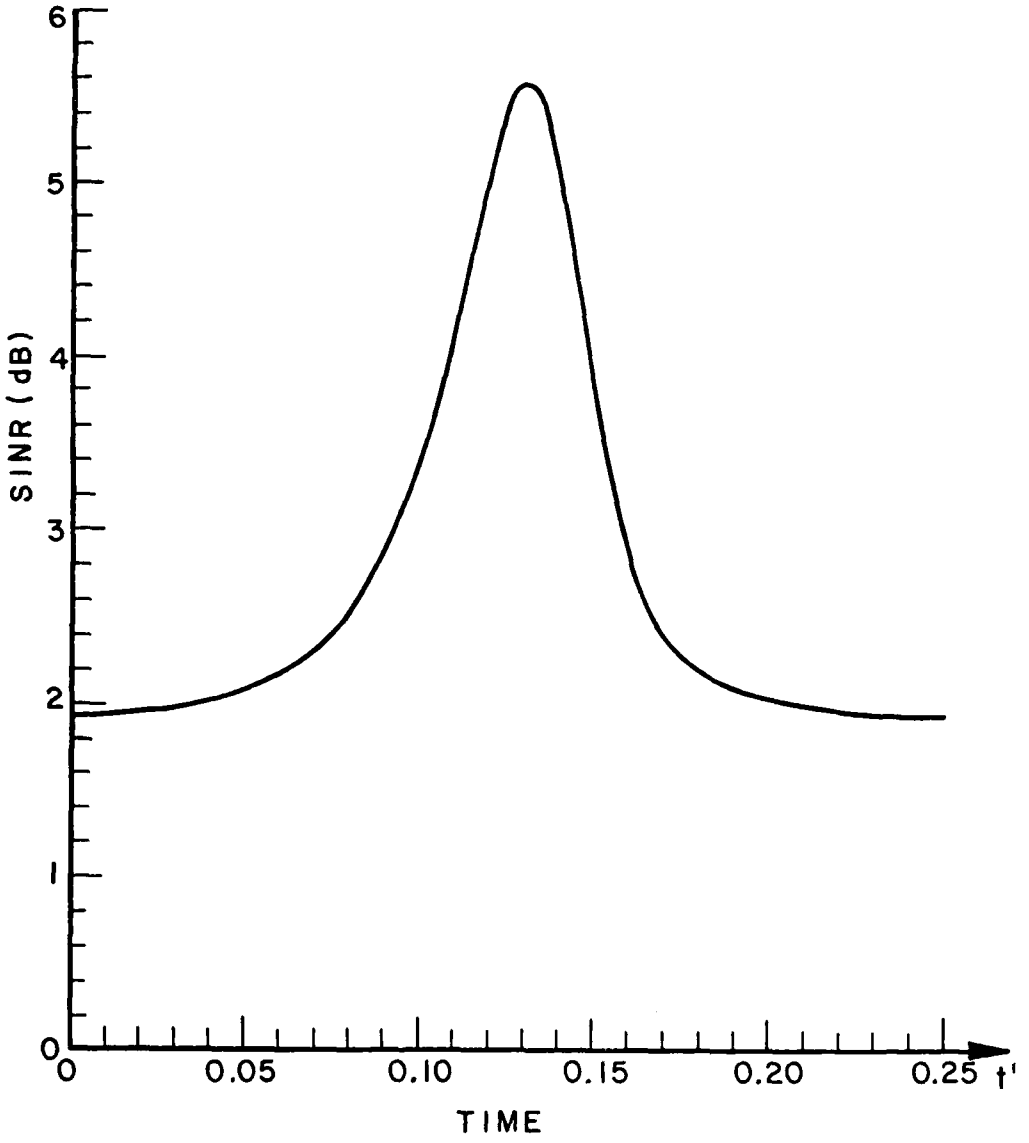

Figure 5. SINR versus time
$\theta_d=0^\circ$, $\theta_i=5^\circ$, $\xi_d=10$ dB,
$\xi_i=20$ dB, $f_m'=2$

close to unity.*

Figures 6 and 7 show typical curves of m and a_{max} as functions of θ_i for $\theta_d=0^o$, $\xi_d=10$ dB and $f_m'=2$. Four different curves are shown, for $\xi_i=5$, 10, 15 and 20 dB. It is seen that m is large and a_{max} is small only when θ_i is close to θ_d. Similar curves for $\theta d \neq 0$ show that the modulation is always small unless $\theta_i \approx \theta_d$.

C. The Effect of Modulation Frequency

The variation m and the peak a_{max} are large at low f_m' and drop as f_m' increases. This result is illustrated in Figures 8 and 9, which show m and a_{max} as a function of frequency f_m' for $\theta_d=0^o$, $\xi_d=0$ dB, $\xi_i=20$ dB, and for several values of θ_i.

This behavior is due to the array speed of response. For low f_m', the array is fast enough to follow the interference modulation. The array pattern changes continuously as the interference power varies. At high f_m', however, the array weights are too slow to keep up with the modulation. Hence, as f_m' is increased, the array weights settle into steady-state values reflecting the time-averaged interference power. As they do so, the desired signal modulation drops.

Figure 8 shows a small dip in m for intermediate values of f_m' for some θ_i. This effect may be seen in the $\theta_i=15^o$ curve, for example. Such behavior is due to the way the shape of the modulation envelope changes as f_m' varies. Figure 10 illustrates this effect. It shows $a_{dn}(t')$ as a function of time for $\theta_i=15^o$ and for two values of f_m', .015 and .04. (In order to plot the two curves on the same graph, we have plotted both versus $f_m't'$.) Figure 10 shows that $a_{max}-a_{min}$ is essentially the same for $f_m'=.04$ as for $f_m'=.015$. However, m is lower at $f_m'=.015$ than at $f_m'=.04$ because a_{max} is higher.

*An exception to this occurs if the interference causes a grating null in the desired signal direction[11]. For isotropic elements a half wavelength apart as considered here, there are no grating nulls.

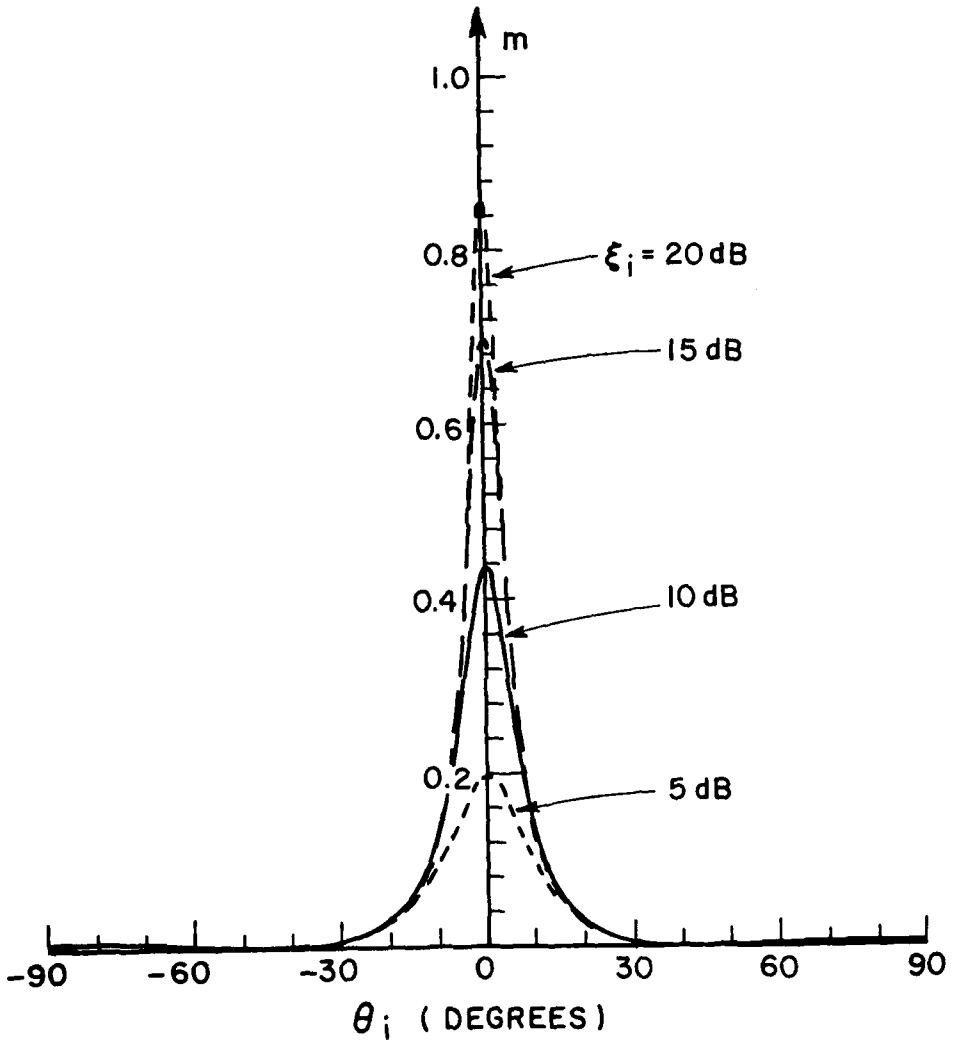

Figure 6. $\underline{m}$ versus θ_i
$\overline{\theta_d=0^o}$, $\xi_d=10$ dB, $f_m'=2$

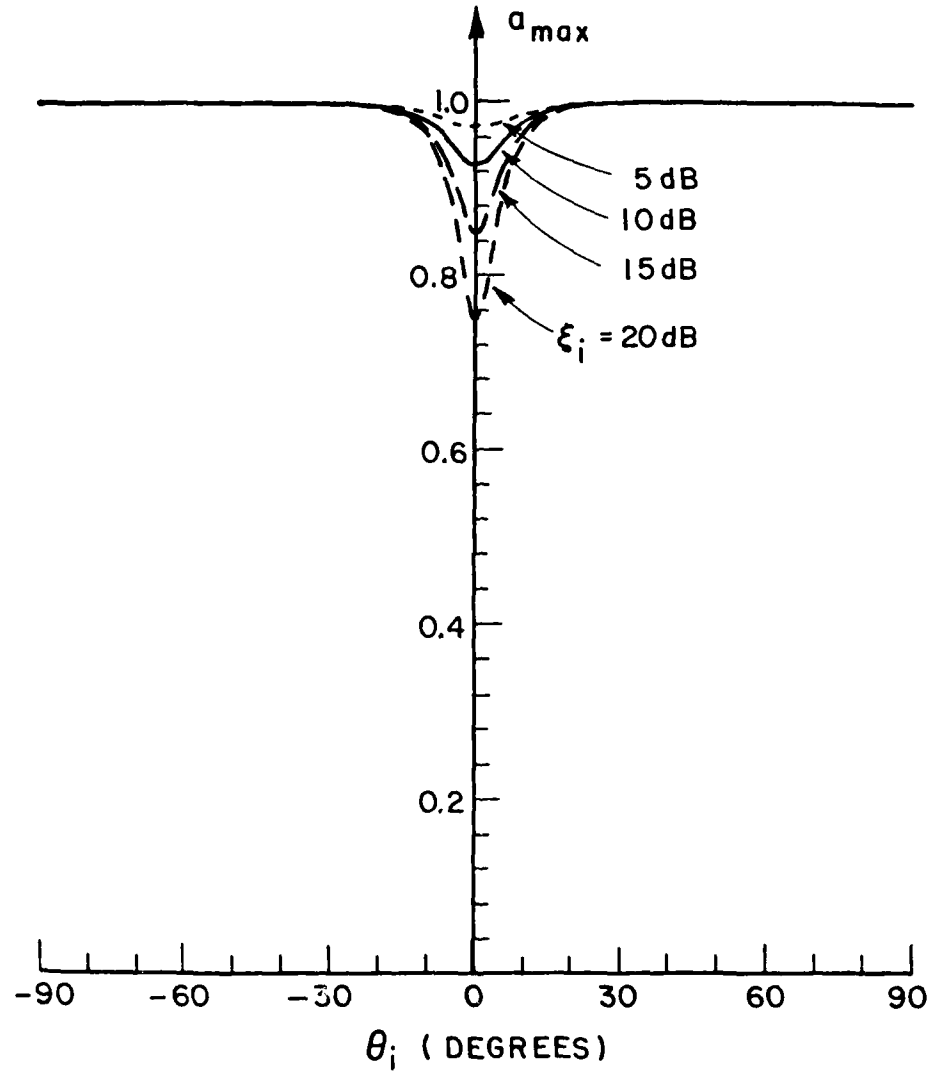

Figure 7. $\frac{a_{max}}{\theta_d=0^\circ,\ \xi_d=10\ dB}$ versus θ_i, $f_m'=2$

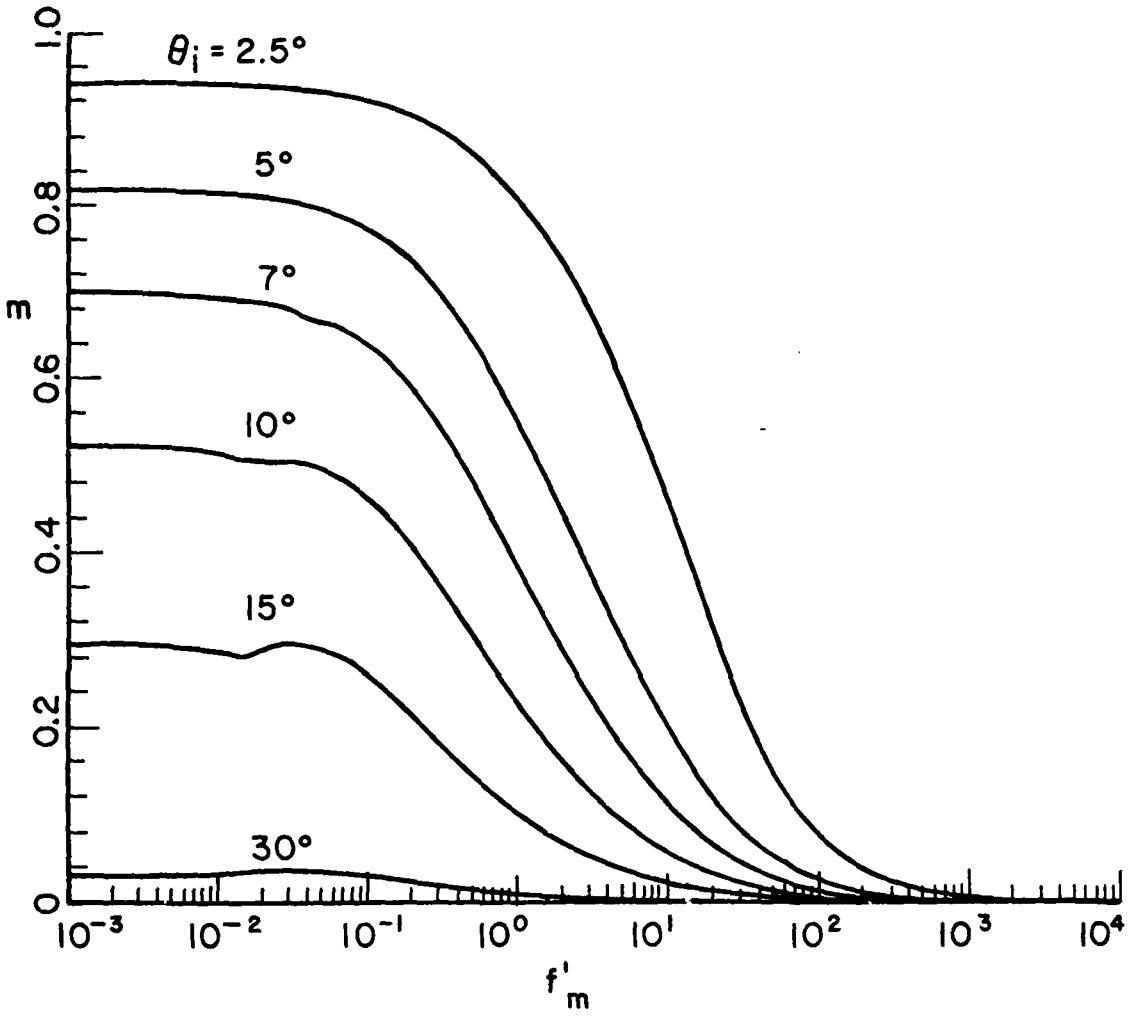

Figure 8. m versus f_m' $\theta_d=0°$, $\xi_d=0$ dB, $\xi_i=20$ dB

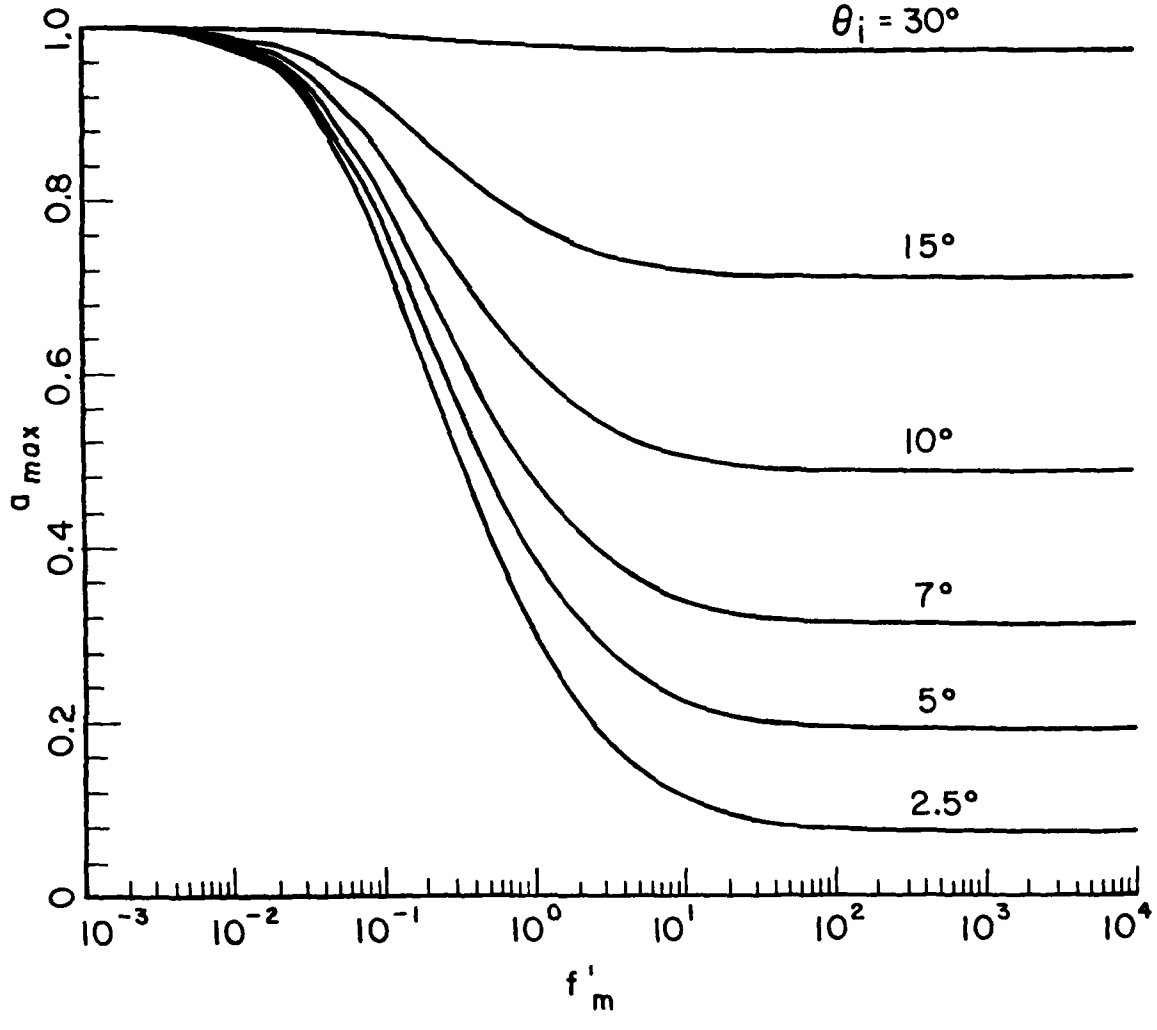

Figure 9. $\frac{a_{max}}{\theta_d=0^\circ}$ versus f_m', $\xi_d=0$ dB, $\xi_i=20$ dB

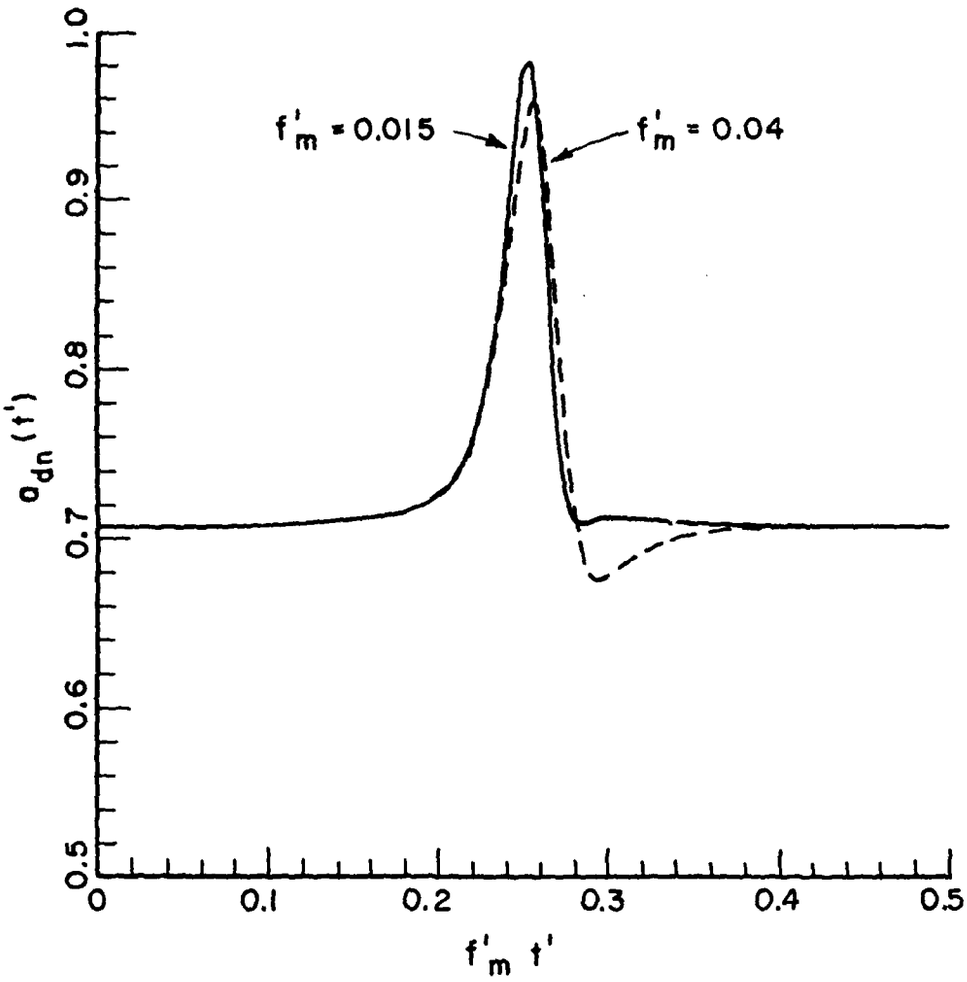

Figure 10. $\frac{a_{dn}(t')}{\theta_d=0^\circ}$ versus time, $\theta_i=15^\circ$, $\xi_d=0$ dB, $\xi_i=20$ dB

D. The Effect of Interference-to-Noise Ratio

For low f_m', the variation m is largest for high INR. For intermediate values of f_m', m peaks at intermediate INR. a_{max} is unity at low f_m' and drops to a minimum value as f_m' increases. The higher the INR, the farther a_{max} drops at high f_m'. Figures 11 and 12 illustrate these results for the case $\theta_d=0^o$, $\theta_i=5^o$, $\xi_d=0$ dB and ξ_i between 0 and 30 dB.

For intermediate f_m', it may be seen in Figure 11 that m peaks at intermediate INR. This behavior is due to the way the modulation envelope changes with INR and to the way m is defined. To illustrate this, Figure 13 shows the modulation envelope $a_{dn}(t')$ over one period for $f_m'=1$ and several INR. It may be seen that $a_{max}-a_{min}$ at first increases with INR but then decreases, because a_{min}, the smallest value of $a_{dn}(t')$ during the cycle, does not drop below about 0.17.

E. The Effect of Desired Signal-to-Noise Ratio

The variation m is largest and the peak a_{max} is smallest for low ξ_d. As ξ_d is increased, m decreases and a_{max} increases.

Figures 14 and 15 illustrate this behavior. Figure 14 shows m and Figure 15 shows a_{max}, both versus f_m' for $\theta_d=0^o$, $\theta_i=5^o$, $\xi_i=20$ dB and for five values of ξ_d between 0 and 20 dB. It is seen that for a given SNR, m peaks slightly at intermediate values of f_m'. This behavior is due to the changes in the shape of the modulation envelope. As an example, Figure 16 shows $a_{dn}(t')$ versus t' for $\xi_d=0$ dB and 10 dB and for $f_m'=.01,.12$ and 10. These values of f_m' span the peak of the curve for $\xi_d=10$ dB in Figure 14 and show how the shape of $a_{dn}(t')$ changes with f_m'. For $\xi_d=0$ dB, the curve of m vs. f_m' in Figure 14 shows no peak, and this behavior is seen in Figure 16.

F. Bit Error Probability

The effect of a time-varying SINR can be evaluated most meaningfully by computing the bit error probability when the array is used in a digital

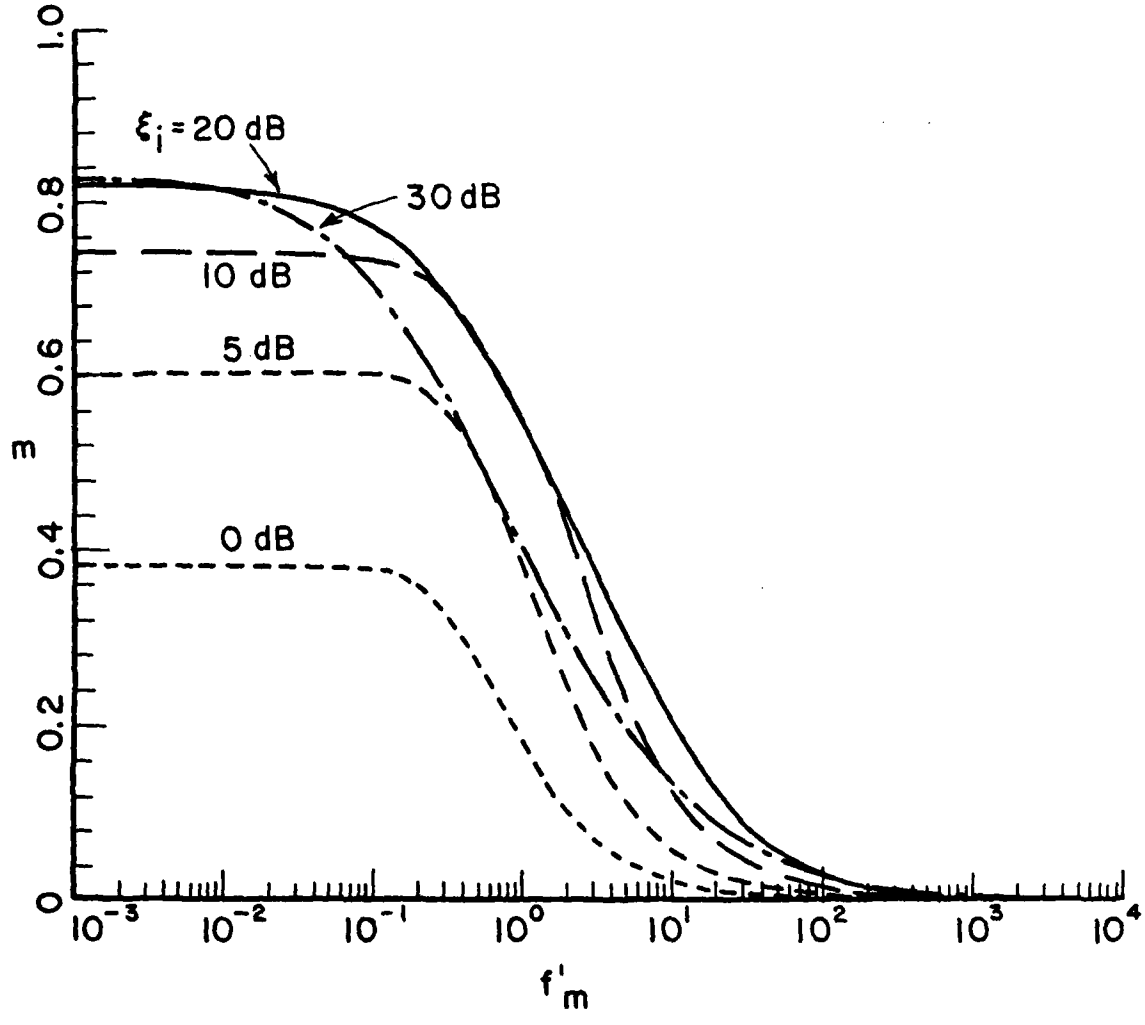

Figure 11. $\frac{m}{\theta_d=0^\circ,\ \theta_i=5^\circ}$ versus f_m', ξ_d=0 dB

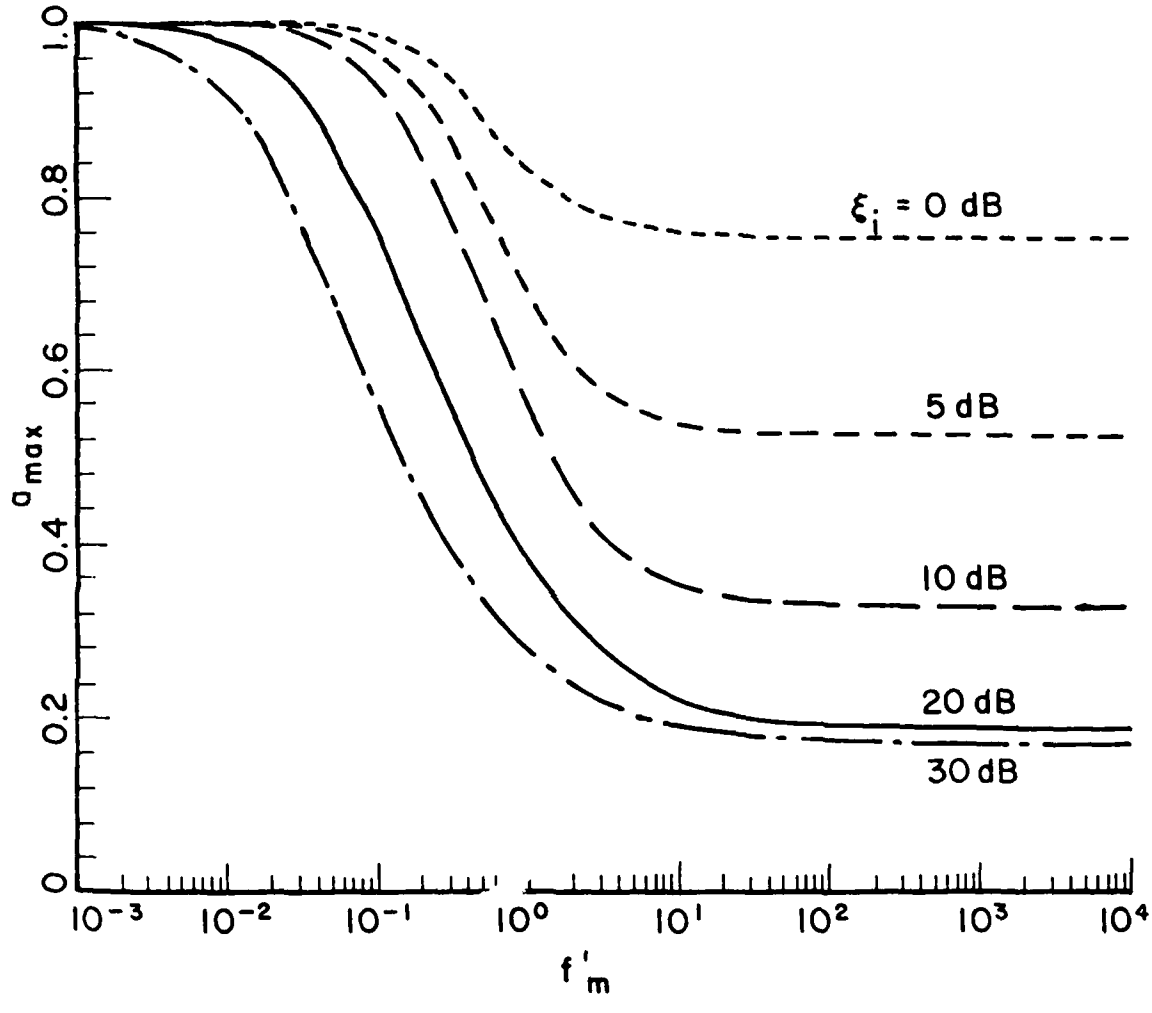

Figure 12. a_{max} versus f_m'
$\theta_d=0^\circ$, $\theta_i=5^\circ$, $\xi_d=0$ dB

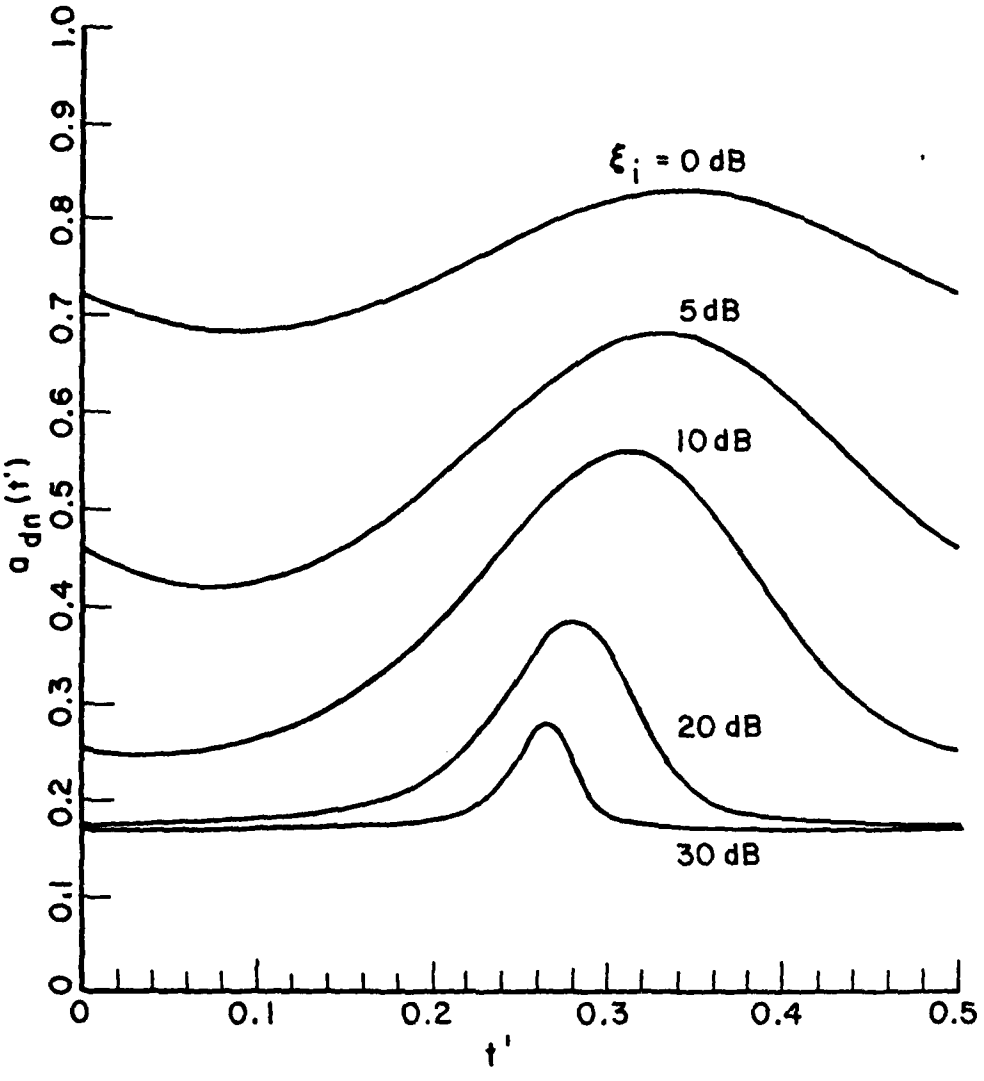

Figure 13. $\frac{a_{dn}(t')}{\theta_d=0^o,\ \theta_i=5^o,\ \xi_d=0\ dB,\ f_m'=1}$ versus time

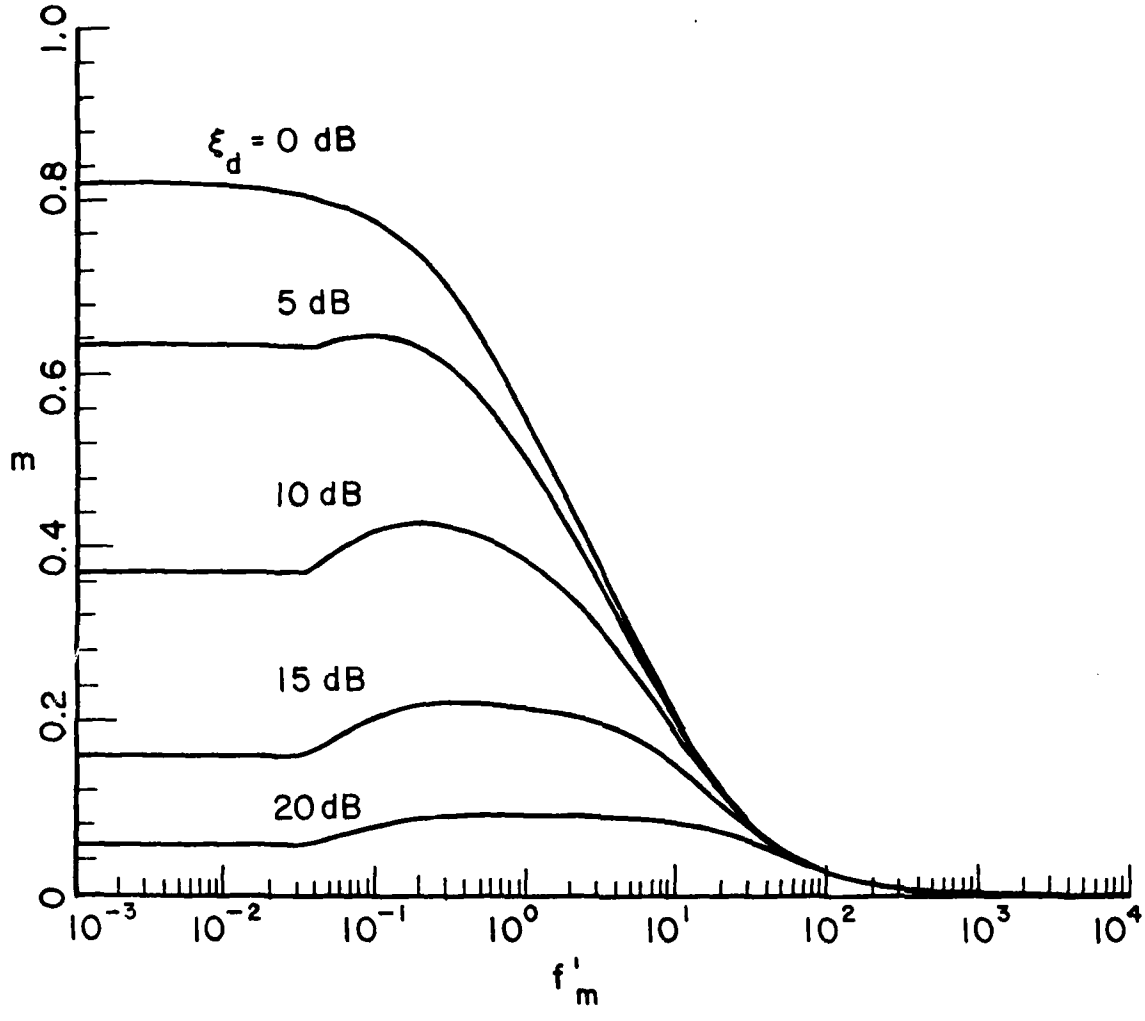

Figure 14. $\underline{m}$ versus $\underline{f_m'}$
$\theta_d=0^o$, $\theta_i=5^o$, ξ_i=20 dB

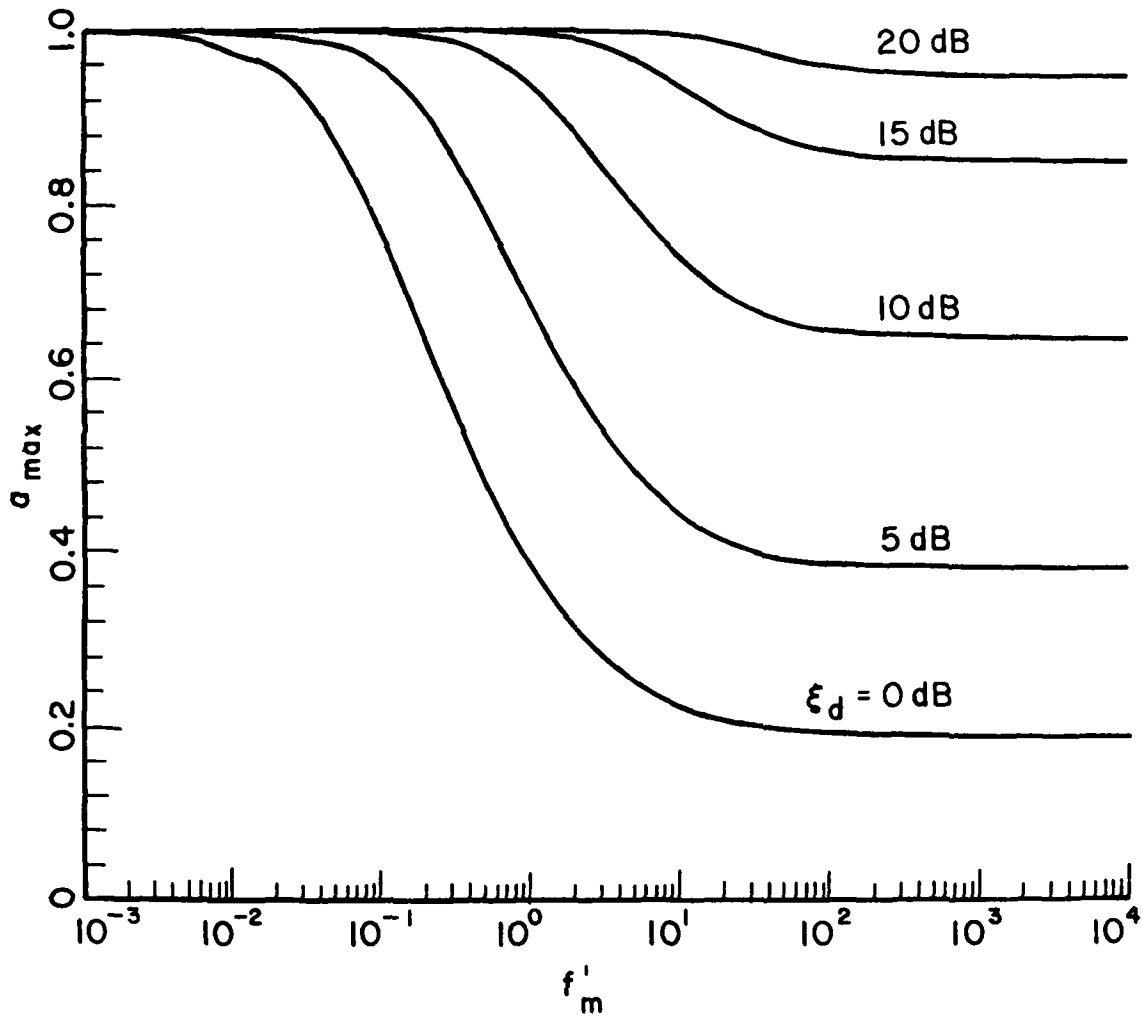

Figure 15. $\frac{a_{max} \text{ versus } f_m'}{\theta_d=0^\circ,\ \theta_j=5^\circ,\ \xi_j=20 \text{ dB}}$

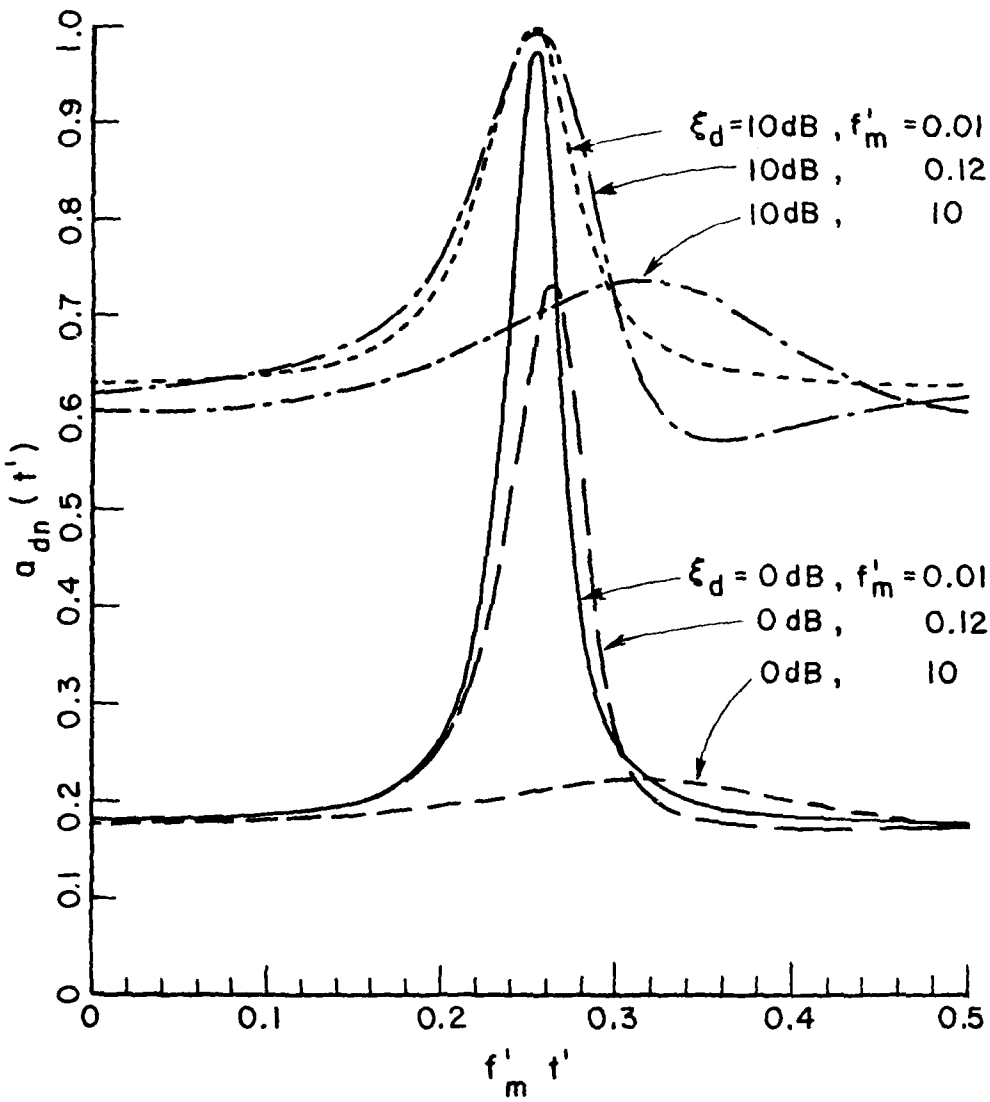

Figure 16. $\frac{a_{dn}(t')}{\theta_d=0^o,\ \theta_i=5^o,\ \xi_i=20\ dB}$ versus $f_m't'$

communication system. For this purpose we arbitrarily assume the desired signal to be a differential phase-shift keyed (DPSK) biphase modulated signal[12]. Also, we assume the reference signal is a replica of the desired signal.*

Because the interference does not produce phase modulation on the desired signal, the only effect of the interference on system performance will be to vary the array output SINR and hence change the bit error probability. For a DPSK signal in white noise, the bit error probability P_e is given by[14]:

$$P_e = (1/2)e^{-E_b/N_o}, \tag{83}$$

where E_b is the signal energy per bit and N_o is the one-sided thermal noise spectral density. For our purposes, it is convenient to express E_b/N_o in terms of signal-to-noise ratio. Since $E_b=P_dT_b$, where P_d is signal power and T_b is the bit duration, and since $1/T_b$ is the effective noise bandwidth, N_o/T_b is the received noise power. Hence,

$$\frac{E_b}{N_o} = \frac{P_d}{(N_o/T_b)} = SNR. \tag{84}$$

In addition, for this analysis we shall assume the interference power at the array output has the same effect on detector performance as thermal noise power. With this assumption, the bit error probability may be written

$$Pe = (1/2)e^{-SINR}. \tag{85}$$

Finally, since the interference causes the SINR to vary periodically, we obtain the effective bit error probability $\overline{P}_e$ by averaging P_e over one period of the interference modulation:

$$\overline{P}_e = 2f_m' \int_0^{(1/2f_m')} (1/2)e^{-SINR(t')}dt'. \tag{86}$$

*As long as the desired signal bandwidth is not excessive, these assumptions produce the same Φ_d as in (19) and the same S as in (23), and hence will yield the same weight behavior as the CW signal assumed above. Moreover, it has been shown that desired signal bandwidth has almost no effect on array performance even if the bandwidth is large[13].

This calculation is valid as long as the bit rate is large compared with the interference modulation period, which we assume to be the case.

Figure 17 shows typical curves of $\overline{P}_e$ as a function of f_m' for $\theta_d=0^o$, $\theta_i=30^o$, $\xi_d=6$ dB and for several values of ξ_i between -20 dB and 30 dB. Figure 18 shows $\overline{P}_e$ versus f_m' for $\theta_d=0^o$, $\xi_d=6$ dB, $\xi_i=20$ dB and for several θ_i between 5^o and 20^o. Both these figures show that f_m' has almost no effect on bit error probability. At low f_m', where the weights can track the interference modulation, the SINR varies over a wider range than at high f_m', where the weights are too slow to follow the modulation. Nevertheless, the average bit error probability is essentially the same for all fm'.

The curves in Figures 17 and 18 show a slight increase in $\overline{P}_e$ as f_m' increases. At high f_m', where the array is too slow to track the interference power variation, the weights are constant. Their values are determined by the time-average interference power, $A_i^2/2$ (see Eq.(20)), or equivalently by the time-average input INR, $\xi_i/2$. In this case one can show that $\overline{P}_e$ has the same value as the bit error probability for an array receiving CW interference with input INR of $\xi_i/2$. $\overline{P}_e$ is slightly lower at low f_m' because in this case the weights track the modulation and yield maximum available SINR for each instantaneous value of interference power. However, the difference between $\overline{P}_e$ at low and high f_m' is so small that, for practical purposes, $\overline{P}_e$ may be considered constant, equal to that for CW interference with INR = $\xi_i/2$.

IV. CONCLUSIONS

We have examined the effect of a sinusoidally modulated (double-sideband, suppressed-carrier) interference signal on the performance of an adaptive array. The major effect of such interference is to cause envelope modulation on the desired signal. This envelope modulation is large only when the interference arrival angle is close to that of the desired signal and when the interference modulation frequency is low relative to the array speed of response. The

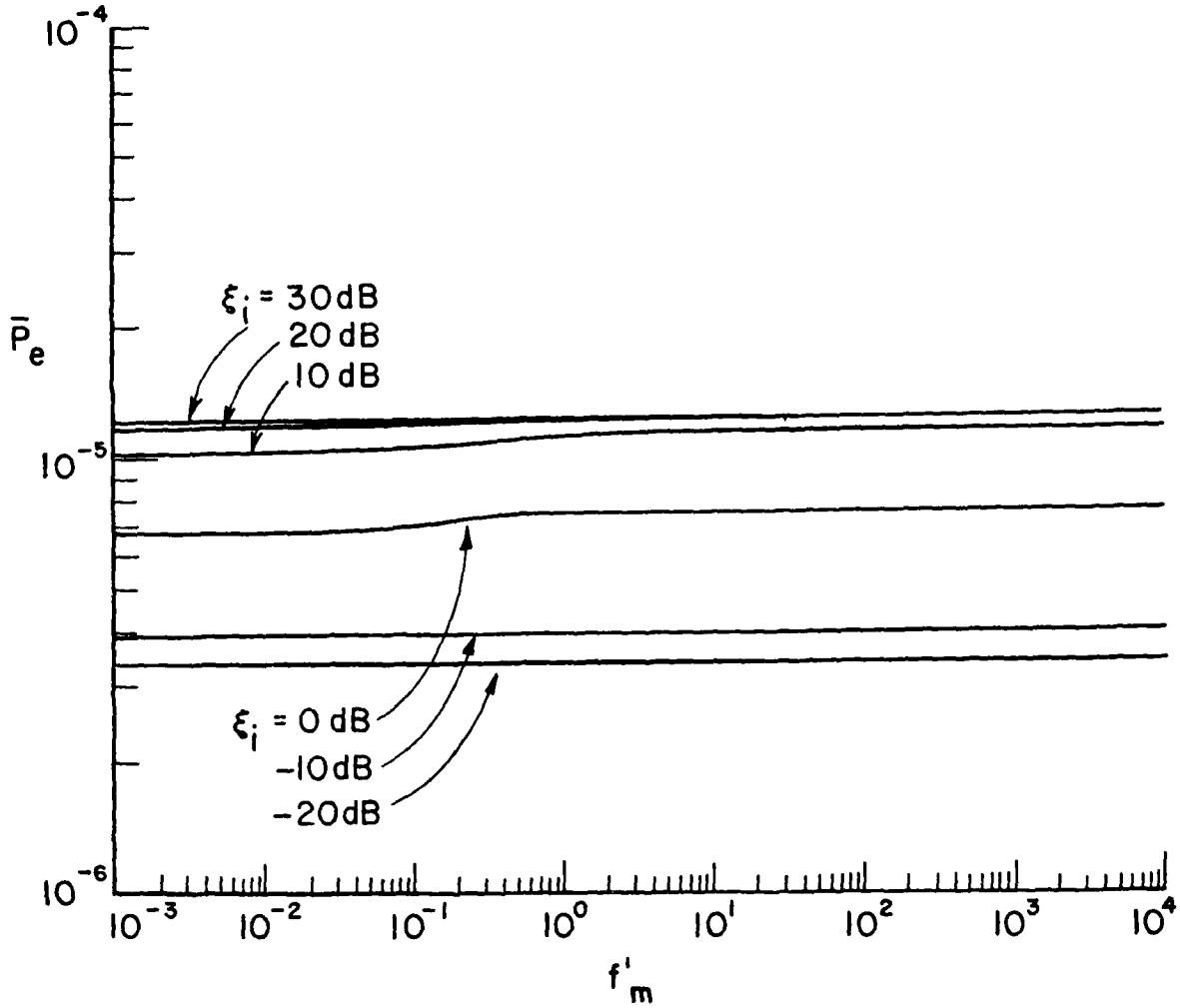

Figure 17. Bit Error Probability versus f_m'
$\theta_d=0^\circ$, $\theta_i=30^\circ$, $\xi_d=6$ dB

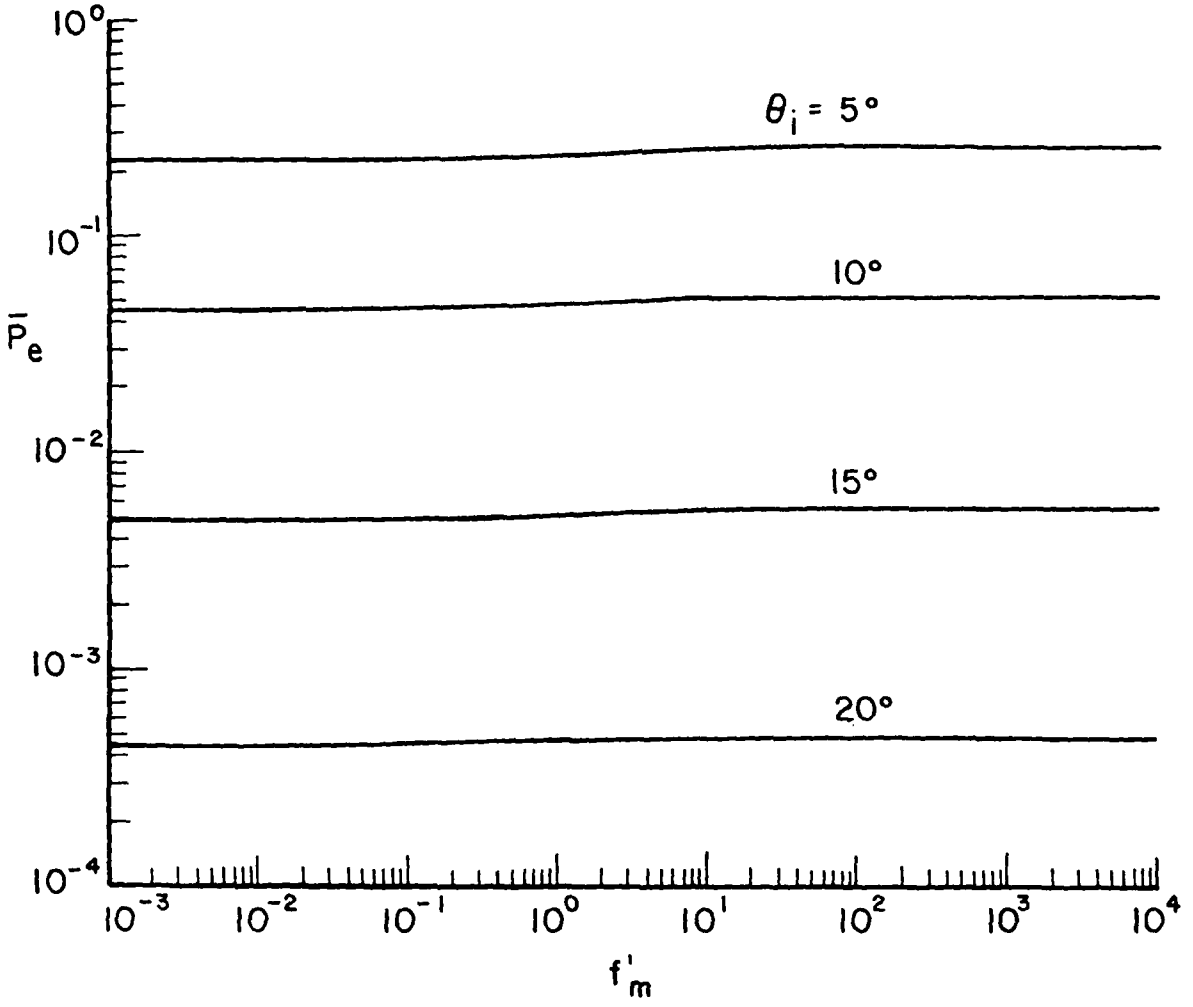

Figure 18. Bit Error Probability versus f_m'
$\theta_d=0^o$, $\xi_d=6$ dB, $\xi_i=20$ dB

envelope modulation is greatest when the interference power is high and the desired signal power is low.

The modulated interference produces no phase modulation on the desired signal. Moreover, if the desired signal is a digital communication signal, such interference results in a bit error probability essentially the same as that for CW interference (from the same angle and with power equal to the time-average power of the modulated interference). Interference modulation frequency has almost no effect on bit error probability.

V. REFERENCES

1. B. Widrow, P. E. Mantey, L. J. Griffiths and B. B. Goode, "Adaptive Antenna Systems," PRoc. IEEE, vol. 55, p. 2143, Dec. 1967.

2. S. P. Applebaum, "Adaptive Arrays," IEEE Trans. Antennas Propagat., vol.AP-24, p.585-598, Sept. 1976.

3. C. A. Baird, Jr. and C. L. Zahm, "Performance Criteria for Narrowband Array Processing," 1971 IEEE Conference on Decision and Control, Miami Beach, Florida, Dec. 15-17, 1971.

4. R. T. Compton, Jr., "The Effect of a Pulsed Interference Signal on an Adaptive Array," to be published in IEEE Transactions on Aerospace and Electronic Systems, vol. 18, no. 3, May 1982.

5. R. L. Riegler and R. T. Compton, Jr., "An Adaptive Array for Interference Rejection," Proc. IEEE, vol. 61, p. 748, June 1973.

6. R. T. Compton, Jr., R. J. Huff, W. G. Swarner and A. A. Ksienski, "Adaptive Arrays for Communication Systems: An Overview of Research at the Ohio State University," IEEE Trans. Antennas Propagat., vol. AP-24, p.599-607, Sept. 1978.

7. R. T. Compton, Jr., "An Adaptive Array in a Spread Spectrum Communication System," Proc. IEEE, vol. 66, p. 289-298, March 1978.

8. H. D'Angelo, Linear Time-Varying Systems: Analysis and Synthesis, Allyn and Bacon, Boston, 1970.

9. P. M. Morse and H. Feshbach, Methods of Theoretical Physics, McGraw-Hill Book Co., New York, 1953; Section 5.2, p. 555ff.

10. R. S. Kennedy, Fading Dispersive Communication Channels, John Wiley and Sons, New York, 1969.

11. A. Ishide and R. T. Compton, Jr., "On Grating Nulls in Adaptive Arrays," IEEE Trans. Antennas Propagat., vol. AP-28, p. 467-475, July 1980.

12. R. E. Ziemer and W. H. Tranter, Principles of Communication, Houghton Mifflin Co., Boston, 1976.

13. W. E. Rodgers and R. T. Compton, JR., "Adaptive Array Bandwidth with Tapped Delay-Line Processing," IEEE Trans. on Aerospace and Electronic Systems, vol. AES-15, p. 21-28, January 1979.

14. W. C. Lindsey and M. K. Simon, Telecommunication Systems Engineering, Prentice-Hall Inc., Englewood Cliffs, N. J., 1973.


DA
FIL
7